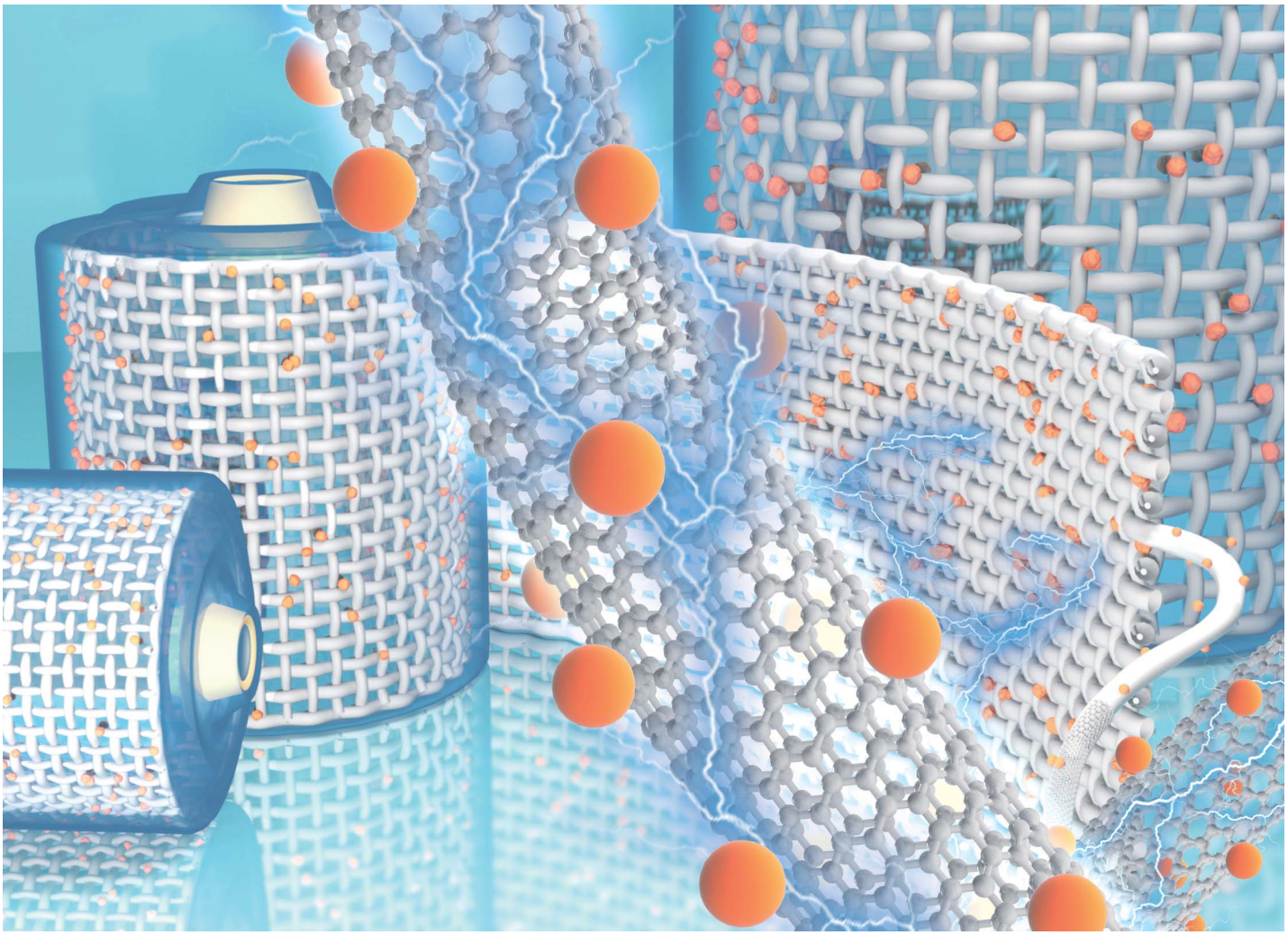

Showcasing a study on the fabrication of flexible anodes from the regenerated-cellulose directed hetero-assembly of nanoparticles and CNTs by Prof. Meifang Zhu at Donghua University and Prof. Yunfeng Lu at UCLA.

Use of regenerated cellulose to direct hetero-assembly of nanoparticles with carbon nanotubes for producing flexible battery anodes

Flexible anodes exhibit the CNT's threaded structure with strong interfacial contact, which provides a shortened lithium-ion diffusion length and continuous electron conduction pathway as well as high mechanical stability, demonstrating a simple and green strategy for the industrial-scale production of energy-storage devices.

As featured in:

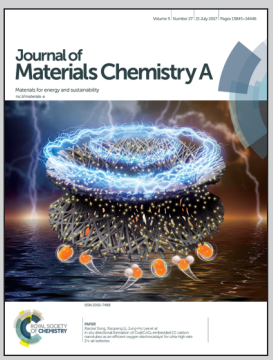

See Meifang Zhu, Yunfeng Lu *et al.*, *J. Mater. Chem. A*, 2017, **5**, 13944.

ROYAL SOCIETY OF CHEMISTRY

rsc.li/materials-a

Registered charity number: 207890

Journal of Materials Chemistry A

COMMUNICATION

View Article Online
View Journal | View Issue

Cite this: J. Mater. Chem. A, 2017, 5, 13944

Received 7th April 2017
Accepted 25th May 2017

DOI: 10.1039/c7ta03043f

rsc.li/materials-a

Use of regenerated cellulose to direct hetero-assembly of nanoparticles with carbon nanotubes for producing flexible battery anodes†

Yanhua Cheng, ‡[ab] Gen Chen, ‡[b] Haobin Wu, [b] Meifang Zhu*[a] and Yunfeng Lu*[b]

Building nanocomposite architectures based on carbon nanotubes (CNTs) and active nanoparticles (NPs) with an engineered interface is of great interest for developing the ability to store electrochemical energy. The use of cellulose to direct hetero-assembly was achieved by *in situ* regenerating an ionic liquid mixture (CNTs, NPs, cellulose) in water, and was applied to the fabrication of flexible anodes consisting of CNTs and NPs. These anodes showed CNTs threading through their structures and exhibited strong interfacial contacts, which provided a relatively short lithium-ion diffusion length and continuous electron conduction pathway as well as high mechanical stability. When evaluated as an anode material for a lithium-ion battery, the flexible nanocomposites showed high reversible capacity and good rate performance compared to traditionally made electrodes, demonstrating a simple and green strategy for the industrial-scale production of energy-storage devices.

Electrochemical redox reactions based on anode materials of lithium-ion batteries generally deliver higher capacity by reacting with more lithium, but at the expense of structural changes including the cracking and pulverization of the electrodes.[1,2] Therefore, finding an excellent support for high-capacity anode materials has long been a focus of the research community.[3,4] Carbon nanotubes (CNTs) are considered to be promising candidates due to their intrinsically high conductivity, high surface area, and excellent mechanical stability.[5] The use of nanocomposite materials made from active nanoparticles (NPs) and CNTs has considerably boosted the performance of currently available energy-storage devices, because these materials improve the ion/electrical conductivity and structural integrity of the devices.[6–10] However, the hetero-assembly of CNTs with NPs is severely hindered by their incompatible interfaces and the poor dispersibility of CNTs in most organic or aqueous solvents.[11,12] Supramolecular chemistry may provide an efficient route for the engineering of nanoscale building blocks, *i.e.*, at the molecular level, as well as of the interface between CNTs and NPs by modification of their surfaces using non-covalent interactions.[13] Polymers such as polyacrylic acid (PAA),[14–17] carboxymethyl cellulose (CMC),[18,19] and alginate[20] have been used as hydrogen-bonding or salt bridges between the hydroxyl groups on the surfaces of NPs and the conductive carbon network to maintain the integrity of the battery electrode during use.[21]

Cellulose is a natural polymer that contains hydroxyl groups in each repeating glucose unit, and the supramolecular structure of cellulose is stabilized by the multiple hydrogen bonds formed by the hydroxyl groups.[22] Cellulose has been demonstrated to be a promising binder for lithium ion battery anodes.[23,24] Compared with petrochemical-derived polymers, cellulose is superior due to its biodegradability, environmental compatibility, and abundance in nature. Ionic liquids (ILs) have been considered as promising solvents for cellulose dissolution and regeneration,[25] which can effectively break and rebuild the extensive hydrogen-bonding networks between cellulose chains.[26] Moreover, imidazolium-based ILs have been applied for the easy dispersion of nanomaterials by forming van der Waals interactions with these nanomaterials.[27,28] Therefore, ILs would be an ideal medium to produce hetero-assembled NP/CNT nanocomposites with controlled architectures and strong interfacial contacts promoted by cellulose.

In the current work, we developed a strategy involving the *in situ* solvation-induced cellulose-assisted formation of a hetero-assembly used for the fabrication of battery anodes. In a typical synthesis, the IL 1-allyl-3-methylimidazolium chloride was used as the solvent, and hydrophilic NP and CNT nanomaterials were used as primary building blocks. As depicted in Fig. 1, cotton (cellulose source) was first dissolved in the IL, followed by the addition of CNTs and NPs to form

[a]State Key Laboratory for Modification of Chemical Fibers and Polymer Materials, College of Materials Science and Engineering, Donghua University, Shanghai, 201620, P. R. China. E-mail: zmf@dhu.edu.cn

[b]Department of Chemical and Biomolecular Engineering, University of California, Los Angeles, CA 90095, USA. E-mail: luucla@ucla.edu

† Electronic supplementary information (ESI) available. See DOI: 10.1039/c7ta03043f

‡ These authors contributed equally to this work.

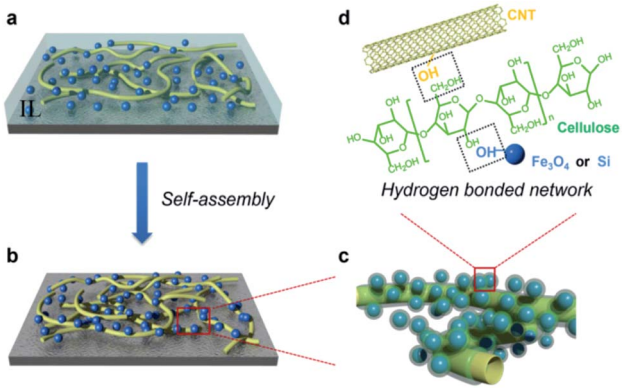

Fig. 1 Schematics illustrating the steps followed to fabricate the NP/CNT composites. (a) The homogenous solution of ILs consisting of cellulose, CNTs and NPs coated on a nickel substrate. (b) The NP/CNT composites formed after the immersion of the IL solution in water. (c) Solvation forces induced the NPs to interact with cellulose and hence assemble around the CNTs. (d) Hydrogen-bonded networks formed between hydroxyl groups of cellulose and the surfaces of the CNTs and NPs.

a homogenous mixture (Fig. 1a). Subsequently, the mixture was coated on a nickel substrate, which was then immersed in water, and the cellulose was regenerated from its IL solution (Fig. 1b). This process induced the NPs to *in situ* assemble around the CNTs using hydrogen-bond interactions between hydroxyl groups (–OH) present in cellulose and on the surfaces of the active materials (Fig. 1c and d). The resulting material was peeled off the substrate to reveal a flexible NP/CNT electrode. This hetero-assembly strategy exhibited several advantages: (i) NPs assembled *in situ* around CNTs when cellulose was regenerated in water when using a one-step process; (ii) a CNT threaded structure enabled effective ion/electron transport; and (iii) regenerated cellulose between CNTs and NPs strengthen the interfacial contacts, ensured the integrity of the electrodes, and finally improved the energy-storage performance. In this study, cellulose played multifunctional roles in serving as a binding agent for NP/CNT nanocomposite architectures. The hydroxyl groups in cellulose that bound the NPs and CNTs together through hydrogen-bonded interactions apparently provided good mechanical integrity for the electrodes.[29] An extensive hydrogen-bonded network in the nanocomposites was proposed to display self-healing feature and hence enable repair of mechanical damage in the electrode during cycling.[1] Moreover, cellulose as a biosourced polymer is promising for use in an efficient large-scale production of energy-storage devices.[23]

The iron oxide (Fe_3O_4) and silicon (Si) NPs were used as active materials, respectively, in this experimental demonstration, owing to their high-energy capacity, low cost, and low toxicity.[30] Adsorption in the range of 3000–3600 cm^{-1} and an intense band at ~1630 cm^{-1}, corresponding to the hydroxyl groups (–OH) on the surfaces of the NPs and CNTs,[31] were observed in the Fourier transform infrared (FTIR) spectra of these materials (Fig. S1†). The NPs, CNTs, and cellulose formed a homogenous solution in ILs (Fig. S2a†). A gel-like integrated structure was then obtained by regenerating the mixture in water (Fig. S2b†). The final form of the regenerated product demonstrated a strong interaction between the components of the composites. The NPs and CNTs were well confined in the composites without leaking into the surrounding water. In this composite, NPs as the energy storage materials provided a shortened lithium-ion diffusion length, while the CNTs offered a pathway for continuous electron conduction. Moreover, cellulose regenerated from water during the solvation process, binds CNTs and NPs to form the hydrogen-bonded interfaces between them, which ensure the integrity of the electrodes upon repeated electrochemical reactions. Therefore, the hetero-assembled composites are expected to deliver a high-storage capability and cycling stability.

Primary Fe_3O_4 NPs were first incorporated into the CNTs and cellulose matrix to form an integrated and flexible anode. The Fe_3O_4 NPs with a face-centered-cubic (fcc) structure were prepared by following the synthetic procedure described previously.[29] Fig. 2a shows a transmission electron microscopy (TEM) image of the NPs, which indicated the individual crystallites to have dimensions of ~10 nm. A high-resolution TEM (HRTEM) image showed a well-crystallized single particle with lattice fringes of 0.25 nm, corresponding to the (311) crystal plane. Fig. 2b shows a scanning electron microscopic (SEM) image of the NP/CNT composites, and clearly showing the Fe_3O_4 NPs clusters to be tangled with CNTs to form a continuous conductive network, which was further confirmed using TEM, as shown in Fig. 2c. An effective coating of cellulose on the Fe_3O_4/CNT surface was observed (Fig. S3†). Cellulose plays an important role in serving as a binding agent to endow the electrodes with good mechanical integrity. Such electrodes with highly entangled components showed flexibility and good mechanical strength, as shown in the inset of Fig. 2d. The electrode with a thickness of 20 μm was indicated from its

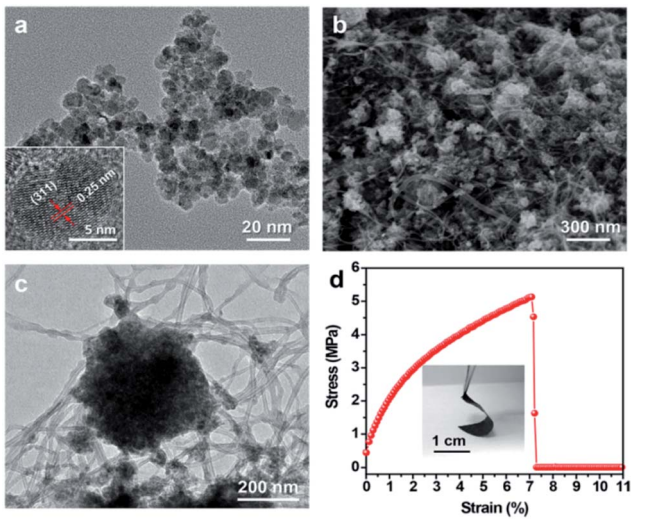

Fig. 2 (a) TEM and HRTEM (inset) image of Fe_3O_4 NPs. (b) SEM image of an Fe_3O_4/CNT electrode with CNT-threaded NP assemblies. (c) TEM image of the Fe_3O_4/CNT composites. (d) Representative stress–strain curve and photograph (inset) of the Fe_3O_4/CNT flexible electrode.

stress–strain curve (Fig. 2d) to exhibit an average tensile strength of 5.2 MPa at a strain of 7.1%, and to display an average elastic modulus of 73 MPa. The flexibility of the electrode was also confirmed by conductivity measurements taken during repeated cycles of bending (Fig. S4†). The good mechanical strength was attributed to the intertwining of the CNTs through the whole composite and the interaction of cellulose with both the CNTs and NPs.

Electrochemical measurements were taken using coin cells with a Li foil used as the counter electrode. Fig. 3a shows representative cyclic voltammetry (CV) curves for the electrode at a sweep rate of 0.5 mV s^{-1} between 0.005 and 3.0 V. In the first cathodic sweep, two peaks at 0.82 and 0.68 V were observed. Such peaks are usually ascribed to the formation of a solid electrolyte interface (SEI), as well as the two steps of the lithiation of Fe_3O_4 (step 1, $Fe_3O_4 + 2Li^+ + 2e^- \rightarrow Li_2Fe_3O_4$; and step 2, $Li_2Fe_3O_4 + 6Li^+ + 6e^- \rightarrow 4Li_2O + 3Fe^0$).[32,33] The broad peak at about 1.8 V in the anodic sweep was attributed to the reversible oxidation of Fe^0 to Fe^{2+} and Fe^{3+}. The subsequent cycles with a cathodic and anodic peak pair at about 0.76 and 1.8 V showed reversible redox reactions ($Fe_3O_4 \leftrightarrow Fe$).[34] The initial peaks at 1.5 and 0.82 V were not observed after the irreversible phase transition of Fe_3O_4 occurring as a result of full lithiation and SEI formation. The positive shift of the cathodic peak to 0.76 V was due to a decreased polarization of the electrode materials relative to that of the first cycle. The above CV results were similar to those of our previous reported work.[29] Fig. 3b shows the charge/discharge curves of the electrode at a current density of 100 mA g^{-1} within a voltage window of 0.005–3.0 V. A voltage plateau appeared at ~0.8 V *versus* Li/Li^+, in good agreement with the above CV results. The initial discharge and charge capacities were 1492 and 758 mA h g^{-1}, respectively. An irreversible loss of capacity is commonly observed for metal oxide anodes and has been attributed to the formation of a solid electrolyte interface (SEI) layer and the decomposition of the electrolyte. The discharge capacity of CNT/Fe_3O_4 composites was well maintained in the following cycles.

Fig. 3c shows the charge/discharge cycling performance of the Fe_3O_4/CNT composites. The composite electrodes benefitted from the interactions of cellulose with both CNTs and NCs through hydrogen bonding, as they showed a stable cycling performance up to 100 cycles of charge/discharge at a current density of 100 mA g^{-1}. From the 10^{th} cycle, the specific capacity kept increasing to 898 mA h g^{-1} after 100 cycles. The gradual increased capacity was attributed to (i) the pulverization of Fe_3O_4 NPs having increased the surface area of the electrode and releasing more active sites for energy storage, and (ii) the reversible growth of the polymeric gel-like film resulting from kinetically activated degradation of the electrolyte.[32,35,36] The coulombic efficiency of the Fe_3O_4/CNT composites was about 100% after the first five cycles. When the current rate was gradually increased at current densities of 100, 250, 500, 750, and 1000 mA g^{-1}, capacities of 730, 537, 461, 392, and 345 mA h g^{-1} were obtained, respectively (Fig. 3d). Control electrodes fabricated by directly mixing Fe_3O_4 NCs with carbon black (CB) and polyvinylidene fluoride (PVDF), and having been formed

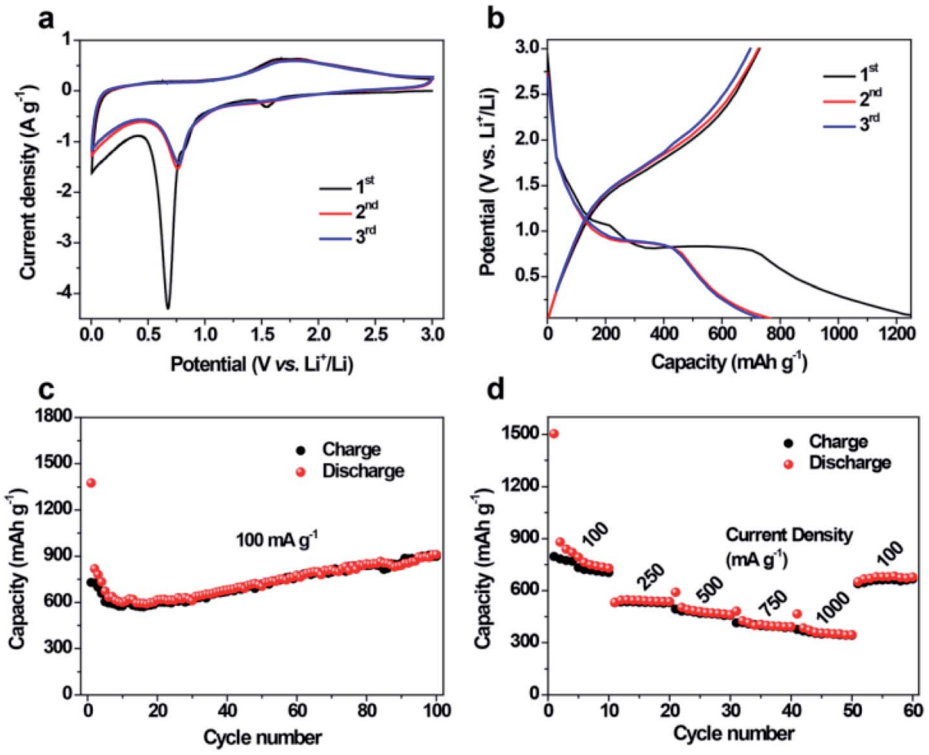

Fig. 3 (a) Representative CV curve of the Fe_3O_4/CNT composite in a potential window of 0.005 to 3 V (*vs.* Li^+/Li) and scan rate of 0.5 mV s^{-1}. (b) The charge and discharge curves of the electrode at a current density of 100 mA g^{-1}. (c) Cycling stability of the composite electrode at a current density of 100 mA g^{-1}. (d) Rate performance of the Fe_3O_4/CNT electrode at various current densities.

using the conventional slurry procedure, showed significantly deteriorated stability (Fig. S5†). Furthermore, the Fe_3O_4/CNT film electrode was assembled into a flexible battery, and still worked well when in a fixed bent state (Fig. S6†). These results confirmed the advantages of using CNT conductive networks to buffer the volume changes and hence stabilize the electrode, and of applying cellulose to serve as a binding agent to form a hydrogen-bonded network in composites and hence ensure the robustness of the structure.

To further understand the electrochemical behavior of the composite electrode during the cycling process, electrochemical impedance spectroscopy (EIS) was conducted along with galvanostatic charge/discharge processes. Nyquist plots of the Fe_3O_4/CNT electrodes at different cycling statuses with an open-circuit voltage (OCV) are shown in Fig. S7a.† The impedance was analyzed by fitting the data points to an equivalent electrical circuit using ZSimpWin software (Fig. S7b†), similar to the circuit employed for other oxide electrodes.[37] The circuit elements were R_e (ohmic resistance of electrolyte and cell components), $R_{sf}||CPE_{sf}$ (impedance of the surface film including the SEI on the electrode, high-frequency semicircle), $R_{ct}||CPE_{dl}$ (charge-transfer impedance due to the electrolyte/surface film/electrode interfaces and the double layer capacitance, medium-frequency semicircle), along with Warburg impedance (W_s) and the intercalation capacitance (C_{int}).[38] The simulated curve and derived data are shown in Fig. S7a and Table S1,† respectively. The fresh cell showed a single broad depressed semicircle in the medium to high frequency region with a resistance of 193 Ω, with these results attributed to the surface film and the charge-transfer resistance (R_{sf} + R_{ct}). After cycling, there was a decrease in total resistance ($R_{sf} + R_{ct} = 97$ Ω). The decreased resistance of the whole battery can be also accounted for the improvement of charge transfer kinetics, resulting in the increase of the capacity during cycling, as shown in Fig. 3c.[32] The structure and morphology of the cycled electrodes were further observed using SEM (Fig. S8†). The SEM image revealed that the electrode still preserved the primary structure with CNTs intertwined in the network, reconfirming the structural integrity. A polymeric coating on the electrode was ascribed to SEI formation.[7]

As a general strategy for the fabrication of hetero-structured anode materials, our solvation-induced self-assembly approach is also applicable to fabricate flexible Si/CNT electrodes. The Si anode material we used showed larger volume changes (~300% volume expansion) with repeated cycling.[39] The commercial Si NPs exhibit a broad size distribution of 50–200 nm, mainly around 100 nm. As shown for the Fe_3O_4/CNT electrodes, the threading of the CNT network through Si clusters was also observed using SEM (Fig. 4a) and TEM (Fig. 4b); these images specifically showed that Si clusters were penetrated by multiple CNTs with intimate interfacial contacts assisted by cellulose (Fig. S9†). The lithium-storage performance of the Si/CNT electrode was also evaluated using coin cells. Fig. 4c shows the first three CV cycles at a potential sweep rate of 0.2 mV s^{-1}. The cathodic peak at 0.73 V on the first CV curve corresponded to the irreversible formation of the SEI layer. The peak disappeared in the following cycles, revealing good stability of such SEI layers in the Si/CNT composites. The voltammetric current associated with the formation of a Li–Si alloy began at ~0.36 V and increased rapidly below 0.18 V, which resulted from the

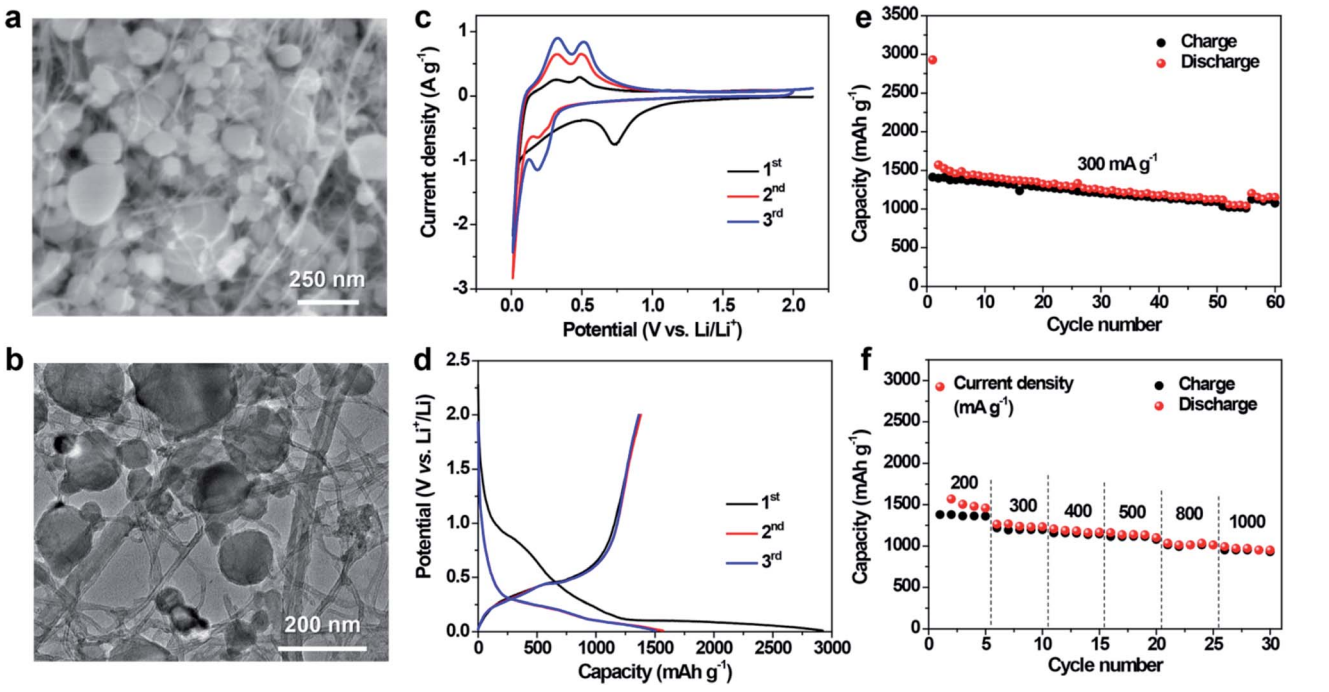

Fig. 4 (a) SEM image and (b) TEM image of Si/CNT composites. (c) Representative CV curve of Si/CNT composite in a voltage range of 0.01 to 2 V (*vs.* Li/Li^+) at scan rate of 0.2 mV s^{-1}. (d) The charge and discharge curves of the electrode at a current density of 200 mA g^{-1}. (e) Cycling stability of the composite electrode at a current density of 300 mA g^{-1}. (f) Rate performance of the Si/CNT electrode at various current densities.

formation of two different phases, specifically those of $Li_{12}Si_7$ and $Li_{15}Si_4$.[40] Two anodic peaks on the first CV curve appeared at about 0.35 V and 0.50 V, accounting for the dealloying of Li ions from Si NPs in the Si/CNT composites. The increase in the charge current with cycling suggested a gradual activation of more active Si NPs embedded inside of the electrode network.[39,41] Fig. 4d shows voltage profiles of the Si/CNT electrode at a current density of 200 mA g^{-1} in the voltage range of 0.01 to 2 V. In the first discharge curve, the small shoulder at 0.9 V was related to SEI formation and/or irreversible Li^+ insertion into the SiO_x impurities.[42] Here, a long extended plateau was observed, corresponding to the formation of amorphous Li_xSi from crystalline Si. The initial discharge and charge capacities were measured to be 2928 and 1380 mA h g^{-1}, respectively. The high irreversible loss of capacity was due to the decomposition of the electrolyte and to the formation of an SEI. After the initial cycle, the discharge capacity of Si/CNT stayed at ~1380 mA h g^{-1}, and the coulombic efficiency increased to 90.7%.

The cycling stability of the composite electrode is displayed in Fig. 4e. This electrode showed a relatively stable cycling performance at a current density of 300 mA g^{-1}. A capacity of 1075 mA h g^{-1}, *i.e.*, about 76% of the initial capacity, was retained after 60 cycles. By comparison, the Si electrode fabricated using the conventional slurry procedure showed severe phase separation, driven by poor interfacial contacts among the constituents in the electrode (Fig. S10†). When assembled in the coin cell, the Si electrode displayed a low capacity, and a much faster decay in capacity, than did the Si/CNT film electrode (Fig. S11†). This result reaffirmed the advantages of the use of regenerated cellulose to induce the integration of Si NPs and CNTs, which facilitated the construction of a 3D interpenetrating Si/CNT network. The Si NPs were encapsulated within a robust conductive framework to enable stable cycling. Benefitting from the hierarchical Si/CNT structure, the flexible electrodes exhibited good rate capabilities. As shown in Fig. 4f, the electrode was able to preserve a capacity of ~950 mA h g^{-1} at a current density of 1 A g^{-1}.

In summary, we have demonstrated a cellulose-directed assembly strategy to fabricate a flexible anode using NPs and CNTs as building blocks. The integrated composites were obtained by *in situ* regenerating the IL mixture in water. The durable electrode performance was attributed to the cellulose-assisted formation of strong interfacial contacts between the NPs and the conductive CNT network. Both Fe_3O_4/CNT and Si/CNT electrodes showed much greater structural integrity than conventional electrodes have shown, and therefore excellent electrochemical performances. The ability to obtain cellulose in a sustainable manner and its ready availability in large quantities from plants contribute to its high promise as a candidate electrode material for practical applications. Moreover, the solvation-induced assembly we deployed offers a simple and green strategy for industrial-scale production of the energy-storage electrodes and may be used for various types of cellulose-based composites.

Acknowledgements

This work was supported by the National Natural Science Foundation (No. 51603035), China Postdoctoral Science Foundation (2016M591572), the Program for Changjiang Scholars and Innovative Research Team in the University (IRT16R13), Science and Technology Commission of Shanghai Municipality (16JC1400700, 17ZR1446300), the Initial Research Funds for Young Teachers of Donghua University, State Key Laboratory for Modification of Chemical Fibers and Polymers Materials.

Notes and references

1 C. Wang, H. Wu, Z. Chen, M. T. McDowell, Y. Cui and Z. Bao, *Nat. Chem.*, 2013, **5**, 1042–1048.
2 J. M. Tarascon and M. Armand, *Nature*, 2001, **414**, 359–367.
3 G. Chen, L. Yan, H. Luo and S. Guo, *Adv. Mater.*, 2016, **28**, 7580–7602.
4 M. Ko, S. Chae, J. Ma, N. Kim, H. W. Lee, Y. Cui and J. Cho, *Nat. Energy*, 2016, **1**, 16113.
5 C. de las Casas and W. Li, *J. Power Sources*, 2012, **208**, 74–85.
6 Z. Chen, Y. Yuan, H. Zhou, X. Wang, Z. Gan, F. Wang and Y. Lu, *Adv. Mater.*, 2014, **26**, 339–345.
7 X. Jia, Y. Cheng, Y. Lu and F. Wei, *ACS Nano*, 2014, **8**, 9265–9273.
8 B. J. Landi, M. J. Ganter, C. D. Cress, R. A. DiLeo and R. P. Raffaelle, *Energy Environ. Sci.*, 2009, **2**, 638–654.
9 Y. Peng, Z. Le, M. Wen, D. Zhang, Z. Chen, H. Bin Wu, H. Li and Y. Lu, *Nano Energy*, 2017, **35**, 44–51.
10 X. Jia, Y. Kan, X. Zhu, G. Ning, Y. Lu and F. Wei, *Nano Energy*, 2014, **10**, 344–352.
11 J. Wang, H. Chu and Y. Li, *ACS Nano*, 2008, **2**, 2540–2546.
12 H. X. Zhang, C. Feng, Y. C. Zhai, K. L. Jiang, Q. Q. Li and S. S. Fan, *Adv. Mater.*, 2009, **21**, 2299–2304.
13 Z. Chen, D. Zhang, X. Wang, X. Jia, F. Wei, H. Li and Y. Lu, *Adv. Mater.*, 2012, **24**, 2030–2036.
14 A. Magasinski, B. Zdyrko, I. Kovalenko, B. Hertzberg, R. Burtovyy, C. F. Huebner, T. F. Fuller, I. Luzinov and G. Yushin, *ACS Appl. Mater. Interfaces*, 2010, **2**, 3004–3010.
15 N. Yabuuchi, K. Shimomura, Y. Shimbe, T. Ozeki, J. Y. Son, H. Oji, Y. Katayama, T. Miura and S. Komaba, *Adv. Energy Mater.*, 2011, **1**, 759–765.
16 B. Koo, H. Kim, Y. Cho, K. T. Lee, N. S. Choi and J. Cho, *Angew. Chem., Int. Ed.*, 2012, **51**, 8762–8767.
17 J. I. Lee, H. Kang, K. H. Park, M. Shin, D. Hong, H. J. Cho, N. R. Kang, J. Lee, S. M. Lee, J. Y. Kim, C. K. Kim, H. Park, N. S. Choi, S. Park and C. Yang, *Small*, 2016, **12**, 3119–3127.
18 J. S. Bridel, T. Azaïs, M. Morcrette, J. M. Tarascon and D. Larcher, *Chem. Mater.*, 2009, **22**, 1229–1241.
19 J. Guo and C. Wang, *Chem. Commun.*, 2010, **46**, 1428–1430.
20 I. Kovalenko, B. Zdyrko, A. Magasinski, B. Hertzberg, Z. Milicev, R. Burtovyy, I. Luzinov and G. Yushin, *Science*, 2011, **334**, 75–79.
21 M. H. Ryou, J. Kim, I. Lee, S. Kim, Y. K. Jeong, S. Hong, J. H. Ryu, T. S. Kim, J. K. Park, H. Lee and J. W. Choi, *Adv. Mater.*, 2013, **25**, 1571–1576.

22 R. P. Swatloski, S. K. Spear, J. D. Holbrey and R. D. Rogers, *J. Am. Chem. Soc.*, 2002, **124**, 4974–4975.
23 L. Jabbour, R. Bongiovanni, D. Chaussy, C. Gerbaldi and D. Beneventi, *Cellulose*, 2013, **20**, 1523–1545.
24 L. Jabbour, C. Gerbaldi, D. Chaussy, E. Zeno, S. Bodoardo and D. Beneventi, *J. Mater. Chem.*, 2010, **20**, 7344–7347.
25 K. M. Gupta and J. Jiang, *Chem. Eng. Sci.*, 2015, **121**, 180–189.
26 S. Zhu, Y. Wu, Q. Chen, Z. Yu, C. Wang, S. Jin, Y. Ding and G. Wu, *Green Chem.*, 2006, **8**, 325–327.
27 M. A. Neouze, *J. Mater. Chem.*, 2010, **20**, 9593–9607.
28 Y. Cheng, Z. Chen, H. Wu, M. Zhu and Y. Lu, *Adv. Funct. Mater.*, 2016, **26**, 1338–1346.
29 Y. Cheng, Z. Chen, M. Zhu and Y. Lu, *Adv. Energy Mater.*, 2015, **5**, 1401207.
30 L. Zhang, H. B. Wu and X. W. Lou, *Adv. Energy Mater.*, 2014, **4**, 1300958.
31 X. C. Shen, X. Z. Fang, Y. H. Zhou and H. Liang, *Chem. Lett.*, 2004, **33**, 1468–1469.
32 J. Luo, J. Liu, Z. Zeng, C. F. Ng, L. Ma, H. Zhang, J. Lin, Z. Shen and H. J. Fan, *Nano Lett.*, 2013, **13**, 6136–6143.
33 C. He, S. Wu, N. Zhao, C. Shi, E. Liu and J. Li, *ACS Nano*, 2013, **7**, 4459–4469.
34 Z. Xiao, Y. Xia, Z. Ren, Z. Liu, G. Xu, C. Chao, X. Li, G. Shen and G. Han, *J. Mater. Chem.*, 2012, **22**, 20566–20573.
35 Y. Wu, Y. Wei, J. Wang, K. Jiang and S. Fan, *Nano Lett.*, 2013, **13**, 818–823.
36 P. Poizot, S. Laruelle, S. Grugeon, L. Dupont and J. M. Tarascon, *Nature*, 2000, **407**, 496–499.
37 M. V. Reddy, T. Yu, C. H. Sow, Z. X. Shen, C. T. Lim, G. V. Subba Rao and B. V. R. Chowdari, *Adv. Funct. Mater.*, 2007, **17**, 2792–2799.
38 N. Sharma, J. Plévert, G. V. Subba Rao, B. V. R. Chowdari and T. J. White, *Chem. Mater.*, 2005, **17**, 4700–4710.
39 Z. Chen, J. W. F. To, C. Wang, Z. Lu, N. Liu, A. Chortos, L. Pan, F. Wei, Y. Cui and Z. Bao, *Adv. Energy Mater.*, 2014, **4**, 1400207.
40 W. Sun, L. Wan, X. Li, X. Zhao and X. Yan, *J. Mater. Chem. A*, 2016, **4**, 10948–10955.
41 Q. Xiao, Y. Fan, X. Wang, R. A. Susantyoko and Q. Zhang, *Energy Environ. Sci.*, 2014, **7**, 655–661.
42 Z. Du, S. Zhang, Y. Liu, J. Zhao, R. Lin and T. Jiang, *J. Mater. Chem.*, 2012, **22**, 11636–11641.